Available online at www.sciencedirect.com
SCIENCE DIRECT®
Journal of Sound and Vibration 273 (2004) 543–568
JOURNAL OF SOUND AND VIBRATION
www.elsevier.com/locate/jsvi

Stability of periodic motion, bifurcations and chaos of a two-degree-of-freedom vibratory system with symmertical rigid stops

G.W. Luo[a,*], J.H. Xie[b]

[a] *School of Mechatronics and Power Engineering, Lanzhou Railway University, Lanzhou 730070, People's Republic of China*
[b] *Department of Applied Mechanics and Engineering, Southwest Jiaotong University, Chengdu 610031, People's Republic of China*

Received 8 July 2002; accepted 6 May 2003

Abstract

A two-degree-of-freedom system having symmetrically placed rigid stops and subjected to periodic excitation is considered. Such models play an important role in the studies of mechanical systems with clearances or gaps. The period-one double-impact symmetrical motion and its Poincaré map are derived analytically. Stability and local bifurcations of the period-one double-impact symmetrical motion are analyzed by the equation of Poincaré map. The routes from period-one double-impact symmetrical motion to chaos, via pitchfork bifurcations and period-doubling bifurcation, are studied by numerical simulation. Some non-typical routes to chaos, caused by grazing the stops and Hopf bifurcation of period two four-impact motion, are analyzed. Hopf bifurcations of period-one double-impact symmetrical and antisymmetrical motions are shown to exist in the two-degree-of-freedom vibratory system with two-sided stops. Interesting feature like the period-one four-impact symmetrical motion is also found, and its route to chaos is analyzed. It is of special interest to acquire an overall picture of the system dynamics for some extreme values of parameters, especially those which relate to the degenerated case of a single-degree-of-freedom system, and these analyses are presented here.

1. Introduction

Vibrating systems with clearances or gaps between the moving parts are frequently encountered in technical applications of mechanism, vehicle traffic and nuclear reactor, etc. Repeated impacts,

*Corresponding author.
E-mail address: luogw@mail.lzjtu.cn (G.W. Luo).

0022-460X/03/$ - see front matter © 2003 Elsevier Ltd. All rights reserved.
doi:10.1016/S0022-460X(03)00512-1

i.e., vibro-impacts, usually occur whenever the components of a vibrating system collide with rigid obstacles or with each other. The principle of operation of vibration hammers, impact dampers, machinery for compacting, milling and forming, shakers, offshore structures, etc., is based on the impact action for moving bodies. With other equipment, e.g., mechanisms with clearances, heat exchangers, fuel elements of nuclear reactors, gears, piping systems, wheel–rail interaction of high-speed railway coaches, etc., impacts also occur, but they are undesirable as they bring about failures, strain, shorter service life and increased noise levels. Researches into vibro-impact problems have important significance on optimization design of machinery with clearances or gaps, noise suppression and reliability analyses, etc. The physical process during impacts is strongly non-linear and discontinuous, but it can be described theoretically and numerically by discontinuities in good agreement with reality. Compared with single impact, the dynamics of vibro-impacts is more complicated, and hence, has received great attention. Many new problems of theory have been advanced in researches into vibro-impacts dynamics, and the study of problems of impacting vibration becomes a new subject on non-linear dynamics. Dynamics of the vibro-impact systems, including global bifurcations [1–5], singularities [6–10] and quasi-periodic impact motions [11–16], etc., have been revealed, and some application researches [17–22] are also unfolded. A two-degree-of-freedom system having symmetrically placed rigid stops and subjected to periodic excitation is considered in the paper. The period-one double-impact symmetrical motion and its Poincaré map are established analytically. Stability and local bifurcations of the period-one double-impact symmetrical motion are analyzed by using the equation of map. The routes from symmetrical periodic impacts to chaos, via pitchfork bifurcation and period-doubling bifurcation, are studied by numerical simulation. Some non-typical routes to chaos, caused by grazing the stops and Hopf bifurcation of period-two four-impact motion, are analyzed. Hopf bifurcation of period-one double-impact symmetrical and antisymmetrical motions are shown to exist in the two-degree-of-freedom vibro-impact system with two-sided stops. It is of special interest to acquire an overall picture of the system dynamics for some extreme values of parameters, especially those which relate to the degenerated case of a single-degree-of-freedom system, and these analyses are presented here.

2. The mechanical model

A two-degree-of-freedom system having symmetrically placed rigid stops and subjected to periodic excitation is shown in Fig. 1. Displacements of the masses M_1 and M_2 are represented by X_1 and X_2, respectively. The masses are connected to linear springs with stiffnesses K_1 and K_2, and linear viscous dashpots with damping constants C_1 and C_2 . The excitations on both masses are harmonic with amplitudes P_1 and P_2. The excitation frequency Ω and the phase τ are the same for both masses. The masses move only in the horizontal direction. For small forcing amplitudes the system will undergo simple oscillations and behave as a linear system. As the amplitude is increased, the mass M_1 eventually begins to hit the stops and the motion becomes non-linear (the other mass is not allowed to impact any rigid stop). The impact is described by a coefficient of restitution R, and it is assumed that the duration of impact is negligible compared to the period of the force. Damping in the mechanical model is assumed as proportional damping of the Rayleigh type, which in this case implies $C_1/K_1 = C_2/K_2$.

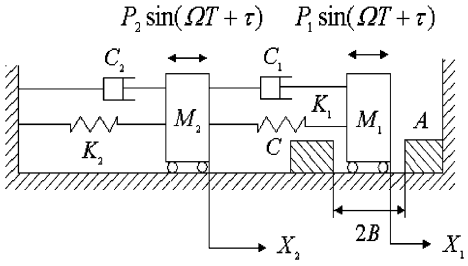

Fig. 1. The schematic of a two-degree-of-freedom vibratory system with symmetrical rigid stops.

The motion processes of the system, between consecutive impacts occurring at the stop A, are considered. Between any two consecutive impacts, the time T is always set to zero directly at the starting point A (the mass M_1 departing from the $X_1 = B$ stop with negative velocity), and the phase angle τ is used only to make a suitable choice for the origin of time in the calculation. The state of the vibro-impact system, immediately after impact, has become new initial conditions in the subsequent process of the motion. Between the stops, the non-dimensional differential equations of motion are given by

$$\begin{bmatrix} 1 & 0 \\ 0 & \dfrac{m_2}{1-m_2} \end{bmatrix} \begin{Bmatrix} \ddot{x}_1 \\ \ddot{x}_2 \end{Bmatrix} + \begin{bmatrix} 2\zeta & -2\zeta \\ -2\zeta & 2\zeta\dfrac{1}{1-c_2} \end{bmatrix} \begin{Bmatrix} \dot{x}_1 \\ \dot{x}_2 \end{Bmatrix} + \begin{bmatrix} 1 & -1 \\ -1 & \dfrac{1}{1-k_2} \end{bmatrix} \begin{Bmatrix} x_1 \\ x_2 \end{Bmatrix} = \begin{Bmatrix} 1-f_{20} \\ f_{20} \end{Bmatrix} \sin(\omega t+\tau), \quad |x_1| < b. \tag{1}$$

When the impacts occur, for $|x_1| = b$, the velocities of the impacting mass M_1 are changed according to the impact law

$$\dot{x}_{1A+} = -R\dot{x}_{1A-} \quad (x_1 = b), \quad \dot{x}_{1C+} = -R\dot{x}_{1C-} \quad (x_1 = -b). \tag{2}$$

In Eqs. (1) and (2), a dot $(\cdot)$ denotes differentiation with to the non-dimensional time t. $\dot{x}_{1A-}$ and $\dot{x}_{1A+}$ ($\dot{x}_{1C-}$ and $\dot{x}_{1C+}$) represent the impacting mass velocities of approach and departure at the instant of impacting with the stop A (C), respectively. Where the non-dimensional quantities

$$m_2 = \frac{M_2}{M_1+M_2}, \quad k_2 = \frac{K_2}{K_1+K_2}, \quad c_2 = \frac{C_2}{C_1+C_2}, \quad f_{20} = \frac{P_2}{P_1+P_2}, \quad \omega = \Omega\sqrt{\frac{M_1}{K_1}},$$
$$t = T\sqrt{\frac{K_1}{M_1}}, \quad \zeta = \frac{C_1}{2\sqrt{K_1M_1}}, \quad b = \frac{BK_1}{P_1+P_2}, \quad x_i = \frac{X_iK_1}{P_1+P_2} \tag{3}$$

have been introduced.

Eqs. (1) and (2) completely determine the dynamics of the system having two-sided constraints. Let $\boldsymbol{\Psi}$ represent the canonical model matrix of Eq. (1). ω_1 and ω_2 denote the eigenfrequencies of the system as impacts do not occur. Taking $\boldsymbol{\Psi}$ as a transition matrix, the equations of motion (1), under the change of variables $\boldsymbol{X} = \boldsymbol{\Psi}\boldsymbol{\xi}$, becomes

$$\boldsymbol{I}\ddot{\boldsymbol{\xi}} + \boldsymbol{C}\dot{\boldsymbol{\xi}} + \boldsymbol{\Lambda}\boldsymbol{\xi} = \bar{\boldsymbol{F}}\sin(\omega t+\delta_k), \tag{4}$$

where $\boldsymbol{X} = (x_1, x_2)^{\mathrm{T}}$, $\boldsymbol{\xi} = (\xi_1, \xi_2)^{\mathrm{T}}$, $\boldsymbol{I}$ is an unit matrix of degree 2×2, $\boldsymbol{C}$ and $\boldsymbol{\Lambda}$ are diagonal matrixs, and $\boldsymbol{C} = \mathrm{diag}[2\zeta\omega_1^2, 2\zeta\omega_2^2]$, $\boldsymbol{\Lambda} = \mathrm{diag}[\omega_1^2, \omega_2^2]$, $\bar{\boldsymbol{F}} = (\bar{f}_1, \bar{f}_2)^{\mathrm{T}} = \boldsymbol{\Psi}^{\mathrm{T}}\boldsymbol{P}_k$, $\boldsymbol{P}_k = (1 - f_{20}, f_{20})^{\mathrm{T}}$, $\boldsymbol{\xi}$ is the response of Eq. (1) in the canonical co-ordinates. The equations of motion (1) are solved by using the modal co-ordinates and the modal matrix approach. The general solution takes the form

$$\begin{aligned} x_i(t) &= \sum_{j=1}^{2} \psi_{ij}(\mathrm{e}^{-\eta_j t}(a_{j1}\cos\omega_{dj}t + b_{j1}\sin\omega_{dj}t) \\ &\quad + A_j\sin(\omega t + \tau) + B_j\cos(\omega t + \tau)), \quad 0 \leqslant t \leqslant t_1, \\ x_i(t) &= \sum_{j=1}^{2} \psi_{ij}(\mathrm{e}^{-\eta_j(t-t_1)}(a_{j2}\cos\omega_{dj}(t-t_1) + b_{j2}\sin\omega_{dj}(t-t_1)) \\ &\quad + A_j\sin(\omega t + \tau) + B_j\cos(\omega t + \tau)), \quad t_1 < t \leqslant t_1 + t_2 \end{aligned} \tag{5}$$

in which, it takes the time t_1 and t_2, respectively, for the mass M_1 to move from the constraint A to C and from the constraint C to A. Where ψ_{ij} are the elements of the canonical modal matrix $\boldsymbol{\Psi}$, $\eta_j = \zeta\omega_j^2$, $\omega_{dj} = \sqrt{\omega_j^2 - \eta_j^2}$, a_j and b_j are the constants of integration which are determined by the initial condition and modal parameters of the system. A_j and B_j are the amplitude parameter, which are given by

$$A_j = \frac{1}{2\omega_{dj}}\left(\frac{\omega + \omega_{dj}}{(\omega + \omega_{dj})^2 + \eta_j^2} - \frac{\omega - \omega_{dj}}{(\omega - \omega_{dj})^2 + \eta_j^2}\right)\bar{f}_j, \tag{6}$$

$$B_j = \frac{\eta_j}{2\omega_{dj}}\left(\frac{1}{(\omega - \omega_{dj})^2 + \eta_j^2} - \frac{1}{(\omega + \omega_{dj})^2 + \eta_j^2}\right)\bar{f}_j. \tag{7}$$

3. Period-one double-impact symmetrical motion

Impacting systems are conveniently studied by use of a mapping derived from the equations of motion. Each iterate of this map corresponds to the mass M_1 striking the stop once. In this section, only the periodic motion of the model, with two symmetrical impacts per force cycle, is considered, which is called the period-one double-impact symmetrical motion. We can choose the Poincaré section $\sigma = \{(x_1, \dot{x}_1, x_2, \dot{x}_2, \theta) \in \mathbf{R}^4 \times \mathbf{S}, x_1 = b, \dot{x}_1 = \dot{x}_{1+}\}$ to establish the Poincaré map of period-one double-impact symmetrical motion

$$\boldsymbol{X}' = \tilde{f}(v, \boldsymbol{X}), \tag{8}$$

where $\theta = \omega t$, $\boldsymbol{X} \in \mathbf{R}^4, v$ is a real parameter, $v \in \mathbf{R}^1$; $\boldsymbol{X} = \boldsymbol{X}^* + \Delta\boldsymbol{X}$, $\boldsymbol{X}' = \boldsymbol{X}^* + \Delta\boldsymbol{X}'$, $\boldsymbol{X}^* = (\dot{x}_{1+}, x_{20}, \dot{x}_{20}, \tau_0)^{\mathrm{T}}$ is a fixed point in the hyperplane σ, $\Delta\boldsymbol{X} = (\Delta\dot{x}_{1+}, \Delta x_{20}, \Delta\dot{x}_{20}, \Delta\tau)^{\mathrm{T}}$ and $\Delta\boldsymbol{X}' = (\Delta\dot{x}'_{1+}, \Delta x'_{20}, \Delta\dot{x}'_{20}, \Delta\tau')^{\mathrm{T}}$ are the disturbed vectors of $\boldsymbol{X}^*$.

Under suitable system parameter conditions, the vibro-impact system given in Fig. 1 can exhibit period-one double-impact symmetrical motion. The symmetrical periodic-impact behavior means that if the dimensionless time t is set to zero directly after an impact occurring at the constraint A, it becomes $2\pi/\omega$ just before the next impact occurring at the same constraint. It takes the same

time for the mass M_1 to move from the constraint A to C and from the constraint C to A, i.e., $t_1 = t_2 = \pi/\omega$. After the origin of θ-co-ordinate is displaced to an impact point o_1, the determination of the period-one double-impact symmetrical motion is based on the fact that they satisfy the following set of periodicity and matching conditions:

$$\begin{aligned}
&x_1(0) = b, \quad x_1(2\pi/\omega) = b, \quad \dot{x}_1(0) = -R\dot{x}_1(2\pi/\omega) = \dot{x}_{1+},\\
&x_2(0) = x_2(2\pi/\omega) = x_{20}, \quad \dot{x}_2(0) = \dot{x}_2(2\pi/\omega) = \dot{x}_{20},\\
&x_1(\pi/\omega) = -b, \quad \dot{x}_{1+}(\pi/\omega) = -R\dot{x}_{1-}(\pi/\omega) = -\dot{x}_{1+},\\
&x_2(\pi/\omega) = -x_2(0) = -x_{20}, \quad \dot{x}_2(\pi/\omega) = -\dot{x}_2(0) = -\dot{x}_{20}.
\end{aligned} \tag{9}$$

Inserting the set of periodicity and matching conditions into the general solutions (5), we can solve for the constants of integration a_{jk}, b_{jk} and the phase angle τ_0. For convenience in the following, we give expression for some symbols h, l_j and $\bar{l}_j$ firstly:

$$l_j = \frac{R\omega_{dj}e_j(e_j + c_j) - (R+1)e_j\eta_j s_j}{1 + e_j c_j} - \omega_{dj} \quad (j = 1, 2), \tag{10}$$

$$\bar{l}_j = \frac{e_j\omega_{dj}(c_j + e_j)}{1 + e_j c_j} + \omega_{dj} \quad (j = 1, 2), \tag{11}$$

$$h = \left(\frac{\psi_{22}\bar{l}_2(R+1)\omega}{\psi_{11}\psi_{22}l_1\bar{l}_2 - \psi_{12}\psi_{21}\bar{l}_1 l_2}\right)\left(\frac{\psi_{12}e_2 s_2}{1 + e_2 c_2}\cdot\frac{\psi_{21}\bar{l}_1}{\psi_{22}\bar{l}_2} - \frac{\psi_{11}e_1 s_1}{1 + e_1 c_1}\right), \tag{12}$$

in which, $s_j = \sin(\pi\omega_{dj}/\omega)$, $c_j = \cos(\pi\omega_{dj}/\omega)$, $e_j = \mathrm{e}^{-\eta_j\pi/\omega}$, $j = 1, 2$.

The phase angle τ_0 of period-one double-impact symmetrical motion is given by

$$\tau_0 = \cos^{-1}\left(\frac{\bar{x}_{10}\gamma \pm \sqrt{\gamma^2 - \bar{x}_{10}^2 + 1}}{\gamma^2 + 1}\right), \tag{13}$$

where

$$\bar{x}_{10} = \frac{b}{hd_2 - d_1}, \quad \gamma = \frac{hd_1 + d_2}{hd_2 - d_1}, \quad d_1 = \sum_{j=1}^{2}\psi_{1j}A_j, \quad d_2 = \sum_{j=1}^{2}\psi_{1j}B_j.$$

The constants of integration a_{jk} and b_{jk} are given by

$$b_{1k} = (-1)^{k-1}\frac{\psi_{22}\bar{l}_2\omega(1+R)(d_1\cos\tau_0 - d_2\sin\tau_0)}{\psi_{11}\psi_{22}l_1\bar{l}_2 - \psi_{12}\psi_{21}\bar{l}_1 l_2}, \tag{14}$$

$$b_{2k} = (-1)^{k}\frac{\psi_{21}\bar{l}_1\omega(1+R)(d_1\cos\tau_0 - d_2\sin\tau_0)}{\psi_{11}\psi_{22}l_1\bar{l}_2 - \psi_{12}\psi_{21}\bar{l}_1 l_2} \quad (k = 1, 2), \tag{15}$$

$$a_{jk} = -\frac{e_j b_{jk} s_j}{1 + e_j c_j} \quad (j = 1, 2). \tag{16}$$

In the paper, we can characterize periodic motions of the vibro-impact system by the symbol $n - p - q$, where q and p is the number of impacts occurring, respectively, at the constraint A and C, and n is the number of the forcing cycles. In formula (13), the sign $\pm$ means that it is possible

to exist two different 1-1-1 symmetrical solutions under the same system parameters for the vibro-impact system with two stops. It should be noted that the existence of 1-1-1 symmetrical orbit requires the condition as below

$$\gamma^2 - \bar{x}_{10}^2 + 1 \geqslant 0, \quad \left| \frac{\bar{x}_{10}\gamma \pm \sqrt{\gamma^2 - \bar{x}_{10}^2 + 1}}{\gamma^2 + 1} \right| \leqslant 1. \tag{17}$$

Otherwise, it is impossible for 1-1-1 symmetrical motion to exist. Substituting the constants of integration (14)–(16) into the general solution (5), we obtain the period-one double-impact symmetrical solution

$$\begin{aligned} x_i(t) &= \sum_{j=1}^{2} \psi_{ij}(\mathrm{e}^{-\eta_j t}(a_{j1}\cos\omega_{dj}t + b_{j1}\sin\omega_{dj}t) \\ &\quad + A_j\sin(\omega t + \tau_0) + B_j\cos(\omega t + \tau_0)), \quad 0 \leqslant t \leqslant \pi/\omega, \\ x_i(t) &= \sum_{j=1}^{2} \psi_{ij}(\mathrm{e}^{-\eta_j (t-t_1)}(a_{j2}\cos\omega_{dj}(t-t_1) + b_{j2}\sin\omega_{dj}(t-t_1)) \\ &\quad + A_j\sin(\omega t + \tau_0) + B_j\cos(\omega t + \tau_0)), \quad t_1 = \pi/\omega, \quad t_1 < t \leqslant 2\pi/\omega. \end{aligned} \tag{18}$$

4. Poincaré map of period-one double-impact symmetrical motion

We consider the perturbed motion of period-one double-impact symmetrical orbit to determine the equation of the map. For convenience in the following, the origin of time is chosen at the impact point. Here let $\tilde{\boldsymbol{X}} = (\tilde{x}_1, \tilde{x}_2)^{\mathrm{T}}$ and $\dot{\tilde{\boldsymbol{X}}} = (\dot{\tilde{x}}_1, \dot{\tilde{x}}_2)^{\mathrm{T}}$ represent displacements and velocities of the perturbed motion, respectively. Between two consecutive impacts occurring at the stop A, the solutions of the perturbed motion are written in the form

$$\begin{aligned} \tilde{x}_i(t) &= \sum_{j=1}^{2} \psi_{ij}(\mathrm{e}^{-\eta_j t}(\tilde{a}_{j1}\cos\omega_{dj}t + \tilde{b}_{j1}\sin\omega_{dj}t) + A_j\sin(\omega t + \tau_0 + \Delta\tau) \\ &\quad + B_j\cos(\omega t + \tau_0 + \Delta\tau)), \quad 0 \leqslant t \leqslant \tilde{t}_1, \\ \tilde{x}_i(t) &= \sum_{j=1}^{2} \psi_{ij}(\mathrm{e}^{-\eta_j (t-\tilde{t}_1)}(\tilde{a}_{j2}\cos\omega_{dj}(t-\tilde{t}_1) + \tilde{b}_j\sin\omega_{dj}(t-\tilde{t}_1)) \\ &\quad + A_j\sin(\omega t + \tau_0 + \Delta\tau) + B_j\cos(\omega t + \tau_0 + \Delta\tau)), \quad \tilde{t}_1 < t \leqslant t_e, \end{aligned} \tag{19}$$

$$\begin{aligned} \dot{\tilde{x}}_i(t) = \sum_{j=1}^{2} \psi_{ij}((\mathrm{e}^{-\eta_j t}(\tilde{b}_{j1}\omega_{dj} - \eta_j\tilde{a}_{j1})\cos\omega_{dj}t - (\eta_j\tilde{b}_{j1} + \tilde{a}_{j1}\omega_{dj})\sin\omega_{dj}t) \\ + A_j\omega\cos(\omega t + \tau_0 + \Delta\tau) - B_j\omega\sin(\omega t + \tau_0 + \Delta\tau)), \quad 0 \leqslant t \leqslant \tilde{t}_1, \end{aligned}$$

$$\dot{\tilde{x}}_i(t) = \sum_{j=1}^{2} \psi_{ij}(\mathrm{e}^{-\eta_j(t-\tilde{t}_1)}((\tilde{b}_{j2}\omega_{dj} - \eta_j\tilde{a}_{j2})\cos\omega_{dj}(t-\tilde{t}_1) - (\eta_j\tilde{b}_{j2} + \tilde{a}_{j2}\omega_{dj})\sin\omega_{dj}(t-\tilde{t}_1)) + A_j\omega\cos(\omega t + \tau_0 + \Delta\tau) - B_j\omega\sin(\omega t + \tau_0 + \Delta\tau)), \quad \tilde{t}_1 < t \leqslant t_e. \tag{20}$$

in which, $\tilde{t}_1 = (\pi/\omega) + \Delta t_1,\ \tilde{t}_2 = (\pi/\omega) + \Delta t_2,\ t_e = \tilde{t}_1 + \tilde{t}_2$.

For the disturbed motion, the dimensionless time is set to zero directly after an impact occurring at the constraint A, it becomes $(2\pi + \Delta\theta)/\omega$ just before the next impact occurring at the same constraint, and $\Delta\theta = \Delta\tau' - \Delta\tau,\ \Delta\theta = \omega(\Delta t_1 + \Delta t_2)$. Letting $t_e = (2\pi + \Delta\theta)/\omega$, the impact boundary conditions of the disturbed motion, occurring, respectively, at the constraint A and C, are expressed by

$$\begin{aligned}
&\tilde{x}_1(0) = b, \quad \tilde{x}_1(t_e) = b, \quad \dot{\tilde{x}}_1(0) = \dot{x}_{1+} + \Delta\dot{x}_{1+}, \quad \tilde{x}_2(0) = x_{20} + \Delta x_{20}, \quad \dot{\tilde{x}}_2(0) = \dot{x}_{20} + \Delta\dot{x}_{20},\\
&\tilde{x}_1(\tilde{t}_{1+}) = -b, \quad \dot{x}_1(\tilde{t}_{1+}) = -\dot{x}_{1+} + \Delta\dot{x}''_{1+}, \quad \tilde{x}_2(\tilde{t}_1) = -x_{20} + \Delta x''_{20}, \quad \dot{\tilde{x}}_2(\tilde{t}_1) = -\dot{x}_{20} + \Delta\dot{x}''_{20},\\
&\tilde{x}_1(\tilde{t}_e) = b, \quad \dot{\tilde{x}}_1(t_{e+}) = \dot{x}_{1+} + \Delta\dot{x}'_{1+}, \quad \tilde{x}_2(t_e) = x_{20} + \Delta x'_{20}, \quad \dot{\tilde{x}}_2(t_e) = \dot{x}_{20} + \Delta\dot{x}'_{20}.
\end{aligned} \tag{21}$$

Inserting the boundary conditions (21) into the perturbed solutions (19) and (20) for $t = 0$, we can solve

$$\tilde{a}_{1k} = \frac{1}{D}(\psi_{22}\tilde{x}_1^{(k)} - \psi_{12}\tilde{x}_2^{(k)} - DA_1\sin\delta_k - DB_1\cos\delta_k), \tag{22}$$

$$\tilde{a}_{2k} = \frac{1}{D}(\psi_{11}\tilde{x}_2^{(k)} - \psi_{21}\tilde{x}_1^{(k)} - DA_2\sin\delta_k - DB_2\cos\delta_k), \tag{23}$$

$$\tilde{b}_{1k} = \frac{1}{D\omega_{d1}}(\psi_{22}(\dot{\tilde{x}}_1^{(k)} + \eta_1\tilde{x}_1^{(k)}) - \psi_{12}(\dot{\tilde{x}}_2^{(k)} + \eta_1\tilde{x}_2^{(k)}) - D(A_1\omega + \eta_1 B_1)\cos\delta_k + D(B_1\omega - \eta_1 A_1)\sin\delta_k), \tag{24}$$

$$\tilde{b}_{2k} = \frac{1}{D\omega_{d2}}(\psi_{11}(\dot{\tilde{x}}_2^{(k)} + \eta_2\tilde{x}_2^{(k)}) - \psi_{21}(\dot{\tilde{x}}_1^{(k)} + \eta_2\tilde{x}_1^{(k)}) - D(A_2\omega + \eta_2 B_2)\cos\delta_k + D(B_2\omega - \eta_2 A_2)\sin\delta_k), \tag{25}$$

in which, $k = 1, 2,\ \tilde{x}_1^{(1)} = b,\ \dot{\tilde{x}}_1^{(1)} = \dot{x}_{1+} + \Delta\dot{x}_{1+},\ \tilde{x}_2^{(1)} = x_{20} + \Delta x_{20},\ \dot{\tilde{x}}_2^{(1)} = \dot{x}_{20} + \Delta\dot{x}_{20},\ \delta_1 = \tau_0 + \Delta\tau,\ \tilde{x}_1^{(2)} = -b,\ \dot{\tilde{x}}_1^{(2)} = -\dot{x}_{1+} + \Delta\dot{x}''_{1+},\ \tilde{x}_2^{(2)} = -x_{20} + \Delta x''_{20},\ \dot{\tilde{x}}_2^{(2)} = -\dot{x}_{20} + \Delta\dot{x}''_{20},\ \delta_2 = \omega\tilde{t}_1 + \tau_0 + \Delta\tau$.

Substituting boundary conditions (21) into the perturbed solution (19) for $t = \tilde{t}_1$, we obtain

$$-b = \sum_{j=1}^{2} \psi_{1j}(\mathrm{e}^{-\eta_j\tilde{t}_1}(\tilde{a}_{j1}\cos\omega_{dj}\tilde{t}_1 + \tilde{b}_{j1}\sin\omega_{dj}\tilde{t}_1) + A_j\sin(\omega\tilde{t}_1 + \tau_0 + \Delta\tau) + B_j\cos(\omega\tilde{t}_1 + \tau_0 + \Delta\tau)) = \tilde{x}_1(\tilde{t}_1). \tag{26}$$

Defining a function $h(\Delta\dot{x}_{1+}, \Delta x_{20}, \Delta\dot{x}_{20}, \Delta\tau, \Delta t_1)$ as

$$h(\Delta\dot{x}_{1+}, \Delta x_{20}, \Delta\dot{x}_{20}, \Delta\tau, \Delta t_1) = \tilde{x}_1(\pi/\omega + \Delta t_1) + b = 0. \tag{27}$$

Suppose $(\partial h/\partial\Delta t_1)_{(0,0,0,0,0)} \neq 0$, according to the implicit function theorem, Eq. (27) can be solved as

$$\Delta t_1 = \Delta t_1(\Delta\dot{x}_{1+}, \Delta x_{20}, \Delta\dot{x}_{20}, \Delta\tau), \quad \Delta t_1(0,0,0,0) = 0. \tag{28}$$

Let $\Delta X = (y_1, y_2, y_3, y_4)^{\mathrm{T}} = (\Delta\dot{x}_{1+}, \Delta x_{20}, \Delta\dot{x}_{20}, \Delta\tau)^{\mathrm{T}}$. The partial derivative of Δt_1 with respect to $\Delta\dot{x}_{1+}$, Δx_{20}, $\Delta\dot{x}_{20}$ and $\Delta\tau$ may be expressed by

$$\frac{\partial \Delta t_1}{\partial y_j} = -\frac{\partial h}{\partial y_j} \Big/ \left(\frac{\partial h}{\partial \Delta t_1}\right), \quad j = 1, 2, 3, 4. \tag{29}$$

Substituting the boundary conditions (21) into the perturbed solutions (19) and (20) for $t = t_e$, we can obtain

$$b = \tilde{x}_1(t_e), \;\; \dot{x}_{1+} + \Delta\dot{x}'_{1+} = -R\dot{\tilde{x}}_1(t_e), \;\; x_{20} + \Delta x'_{20} = \tilde{x}_2(t_e), \;\; \dot{x}_{20} + \Delta\dot{x}'_{20} = \dot{\tilde{x}}_2(t_e). \tag{30}$$

Defining a function $g(\Delta\dot{x}_{1+}, \Delta x_{20}, \Delta\dot{x}_{20}, \Delta\tau, \Delta t_1, \Delta t_2)$ as

$$g(\Delta\dot{x}_{1+}, \Delta x_{20}, \Delta\dot{x}_{20}, \Delta\tau, \Delta t_1, \Delta t_2) = \tilde{x}_1(t_e) - b = 0. \tag{31}$$

Suppose $(\partial g/\partial \Delta t_2)_{(0,0,0,0,0,0)} \neq 0$, according to the implicit function theorem, Eq. (31) can be solved as

$$\Delta t_2 = \Delta t_2(\Delta\dot{x}_{1+}, \Delta x_{20}, \Delta\dot{x}_{20}, \Delta t_1, \Delta\tau), \quad \Delta t_2(0, 0, 0, 0, 0) = 0. \tag{32}$$

The partial derivative of Δt_2 to $\Delta\dot{x}_{1+}$, Δx_{20}, $\Delta\dot{x}_{20}$ and $\Delta\tau$ may be expressed by

$$\frac{\partial \Delta t_2}{\partial y_j} = -\left(\frac{\partial g}{\partial y_j} + \frac{\partial g}{\partial \Delta t_1} \cdot \frac{\partial \Delta t_1}{\partial y_j}\right) \Big/ \left(\frac{\partial g}{\partial \Delta t_2}\right), \quad j = 1, 2, 3, 4. \tag{33}$$

Inserting formulae (28) and (32) into formula (30), we get finally the Poincaré map of period-one double-impact symmetrical motion

$$\begin{aligned}
\Delta\dot{x}'_{1+} &= \tilde{f}_1(\Delta\dot{x}_{1+}, \Delta x_{20}, \Delta\dot{x}_{20}, \Delta\tau, \Delta t_1, \Delta t_2) - \dot{x}_{1+} \overset{\text{Def}}{=} f_1(\Delta\dot{x}_{1+}, \Delta x_{20}, \Delta\dot{x}_{20}, \Delta\tau), \\
\Delta x'_{20} &= \tilde{f}_2(\Delta\dot{x}_{1+}, \Delta x_{20}, \Delta\dot{x}_{20}, \Delta\tau, \Delta t_1, \Delta t_2) - x_{20} \overset{\text{Def}}{=} f_2(\Delta\dot{x}_{1+}, \Delta x_{20}, \Delta\dot{x}_{20}, \Delta\tau), \\
\Delta\dot{x}'_{20} &= \tilde{f}_3(\Delta\dot{x}_{1+}, \Delta x_{20}, \Delta\dot{x}_{20}, \Delta\tau, \Delta t_1, \Delta t_2) - \dot{x}_{20} \overset{\text{Def}}{=} f_3(\Delta\dot{x}_{1+}, \Delta x_{20}, \Delta\dot{x}_{20}, \Delta\tau), \\
\Delta\tau' &= \Delta\tau + \omega\Delta t_1 + \omega\Delta t_2 \overset{\text{Def}}{=} f_4(\Delta\dot{x}_{1+}, \Delta x_{20}, \Delta\dot{x}_{20}, \Delta\tau).
\end{aligned} \tag{34}$$

The Poincaré map (34) may be expressed briefly by

$$\Delta\boldsymbol{X}' = \tilde{f}(v, \boldsymbol{X}) - \boldsymbol{X}^* \overset{\text{Def}}{=} f(v, \Delta\boldsymbol{X}), \tag{35}$$

where $f(v, \Delta\boldsymbol{X}) = (f_1, f_2, f_3, f_4)^{\mathrm{T}}$, $\Delta\boldsymbol{X} = (\Delta\dot{x}_{1+}, \Delta x_{20}, \Delta\dot{x}_{20}, \Delta\tau)^{\mathrm{T}}$ and $\Delta\boldsymbol{X}' = (\Delta\dot{x}'_{1+}, \Delta x'_{20}, \Delta\dot{x}'_{20}, \Delta\tau')^{\mathrm{T}}$ are the disturbed vectors of the fixed point $\boldsymbol{X}^*$ of 1-1-1 symmetrical motion.

Linearizing the Poincaré map at the fixed point $\boldsymbol{X}^* = (\dot{x}_{1+}, x_{20}, \dot{x}_{20}, \tau_0)^{\mathrm{T}}$ results in the matrix

$$D\boldsymbol{f}(v,0) = \begin{pmatrix} \dfrac{\partial f_1}{\partial \Delta \dot{x}_{1+}} & \dfrac{\partial f_1}{\partial \Delta x_{20}} & \dfrac{\partial f_1}{\partial \Delta \dot{x}_{20}} & \dfrac{\partial f_1}{\partial \Delta \tau} \\ \dfrac{\partial f_2}{\partial \Delta \dot{x}_{1+}} & \dfrac{\partial f_2}{\partial \Delta x_{20}} & \dfrac{\partial f_2}{\partial \Delta \dot{x}_{20}} & \dfrac{\partial f_2}{\partial \Delta \tau} \\ \dfrac{\partial f_3}{\partial \Delta \dot{x}_{1+}} & \dfrac{\partial f_3}{\partial \Delta x_{20}} & \dfrac{\partial f_3}{\partial \Delta \dot{x}_{20}} & \dfrac{\partial f_3}{\partial \Delta \tau} \\ \dfrac{\partial f_4}{\partial \Delta \dot{x}_{1+}} & \dfrac{\partial f_4}{\partial \Delta x_{20}} & \dfrac{\partial f_4}{\partial \Delta \dot{x}_{20}} & \dfrac{\partial f_4}{\partial \Delta \tau} \end{pmatrix}_{(v,0,0,0,0)}. \tag{36}$$

Let $\Delta \boldsymbol{X} = (y_1, y_2, y_3, y_4)^{\mathrm{T}} = (\Delta \dot{x}_{1+}, \Delta x_{20}, \Delta \dot{x}_{20}, \Delta \tau)^{\mathrm{T}}$, the elements of the matrix are given by

$$\frac{\partial f_j}{\partial y_i} = \frac{\partial \widetilde{f}_j}{\partial y_i} + \frac{\partial \widetilde{f}_j}{\partial \Delta t_1} \cdot \frac{\partial \Delta t_1}{\partial y_i} + \frac{\partial \widetilde{f}_j}{\partial \Delta t_2} \cdot \frac{\partial \Delta t_2}{\partial y_i} \quad (i,j = 1,2,3,4). \tag{37}$$

If the map $\tilde{f}(v, \boldsymbol{X})$ has a fixed point then the vibro-impact system shown in Fig. 1 has a periodic orbit with two symmetrical impacts per force cycle. If none of the eigenvalues of the matrix $D\boldsymbol{f}(v_0, 0)$ lie on the unit circle or outside it, then it can be shown that $\tilde{f}(v, \boldsymbol{X})$ has essentially the same behavior as $\tilde{f}(v_0, \boldsymbol{X})$ for $|v - v_0|$ small. Suppose that for $v = v_0$, the system has a stable period-one double-impact symmetrical solution $\boldsymbol{X}^*(t)$. Hence in this case, for $|v - v_0|$ small, the solutions of the vibro-impact system near $\boldsymbol{X}^*(t)$ have stable period-one double-impact symmetrical behavior as $v = v_0$. If the eigenvalues of $D\boldsymbol{f}(v, 0)$ with the largest modules lie on the unit circle when $v = v_c$ (v_c is a bifurcation value) then there is the possibility of bifurcations taking place. In general, bifurcations occur in various ways according to the numbers of the eigenvalues on the unit circle and their position on the unit circle, resulting in qualitative changes of the system dynamics. If $D\boldsymbol{f}(v, 0)$ has a pair of complex conjugate eigenvalues, crossing the unit circle as v passes through v_c; the remainder of the spectrum of $D\boldsymbol{f}(v, 0)$ will be assumed to stay strictly inside the unit circle, Hopf bifurcation associated with period-one double-impact symmetrical motion may take place and it is discussed in Section 6 of this paper. If $D\boldsymbol{f}(v, 0)$ has a real eigenvalue, crossing the unit circle from the point $(-1, 0)$ or point $(+1, 0)$ as v passes v_c; the remainder of the spectrum of $D\boldsymbol{f}(v, 0)$ are strictly inside the unit circle, period-doubling or pitchfork bifurcation of period-one double-impact symmetrical motion can occur respectively and a detailed discussion of them follows in Section 5 of this paper.

It should be mentioned that the existence condition (17) is stronger in the comparison with stability conditions. It means that theoretically stable 1-1-1 symmetrical motion can not really exist when the existence condition is not met.

5. Pitchfork bifurcation, period-doubling bifurcation and grazing singularity

The existence and stability of period-one double-impact symmetrical motion were found explicitly in this section. Also, local bifurcations at the points of change in stability were considered, thus giving some information about the existence of other types of motions, such as pairs of antisymmetrical orbits. The vibro-impact system, with system parameters

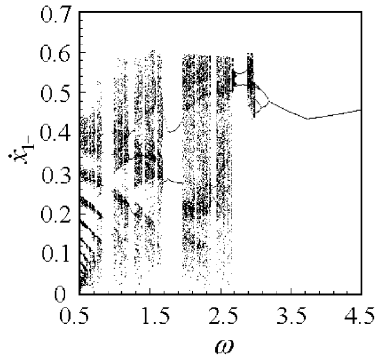

Fig. 2. The global bifurcation diagram of 1-1-1 motion.

(1): $m_2 = 0.6667$, $k_2 = 0.8333$, $\zeta = 0.05$, $R = 0.8$, $f_{20} = 0$ and $b = 0.1$, has been chosen for analysis. The forcing frequency ω is taken as a control parameter. The eigenvalues of $Df(\omega, 0)$ are computed with $\omega \in [3.3, 4.0]$. All eigenvalues of the matrix $Df(\omega, 0)$ still stay inside the unit circle with $\omega \in (3.716972, 4]$. As $\omega = \omega_c = 3.716972$, $Df(\omega, 0)$ has a real eigenvalue $\lambda_1(\omega_c)$ at the point (1,0) of the unit circle in the complex plane, while all other eigenvalues $\lambda_i(\omega_c)$ $(i = 2, 3, 4)$ are still inside the unit circle. The real eigenvalue $\lambda_1(\omega_c)$ will escape the unit circle from the point (1,0), and the other eigenvalues will stay still inside the unit circle, as ω passes through $\omega_c = 3.716972$ decreasingly. Pitchfork bifurcation of period-one double-impact symmetrical motion occurs in this case.

The above-mentioned analysis is verified by presentation of numerical results for the two-degree-of-freedom system with symmetrical rigid stops. The Poincaré section is taken in the form $\sigma = \{(x_1, \dot{x}_1, x_2, \dot{x}_2, \theta) \in \mathbf{R}^4 \times \mathbf{S},\ x_1 = b, \dot{x}_1 = \dot{x}_{1+}\}$. Numerical analyses are carried out for determining the dynamical responses of the vibro-impact system. In Fig. 2 results from the simulation are shown for system parameters (1), and ω varying in the range [0.5, 4.5]. Impact velocities at the stop A are shown versus ω. Some periodic response and phase plane portraits of the mass M_1 are plotted in Figs. 3 and 4, respectively. It is shown, by the numerical results, that the system can exhibit stable period-one double-impact symmetrical motion with $\omega \in (3.716972, 4.5]$. The stable responses and phase plane portrait of period-one double-impact symmetrical motion are plotted for $\omega = 4.0$ in Fig. 3. As ω is decreased from $\omega_c = 3.716972$, the 1-1-1 symmetrical motion has changed its stability, and pitchfork bifurcation of 1-1-1 symmetrical motion occurs so that a pair of antisymmetrical double-impact orbits are born, as seen in Figs. 4(a) and (b). Two 1-1-1 antisymmetrical orbits, caused by different initial conditions, are represented, respectively, by real lines and dotted lines in Figs. 4(a) and (b). The analysis of stability and local bifurcation of period-one double-impact symmetrical motion is supported well by the numerical results. With further decrease in parameter ω, the 1-1-1 antisymmetrical motions will lose stability, these motions then each undergo a succession of period doubling bifurcations, which eventually result in apparently non-periodic, or chaotic motions. The 2-2-2 impact motion, 4-4-4 impact motion, 8-8-8 impact motion and chaos of the mass M_1 are plotted, respectively, in the form of phase plane portraits, for $\omega = 3.1$, $\omega = 3.029$, $\omega = 2.989$ and $\omega = 2.98$ in Figs. 4(c)–(f).

When the mass M_1 arrives at the right stop A with zero velocity $\dot{x}_1 = 0$, a "grazing" bifurcation will occur, which causes singularity of the impact map. The Poincaré map of the vibro-impact

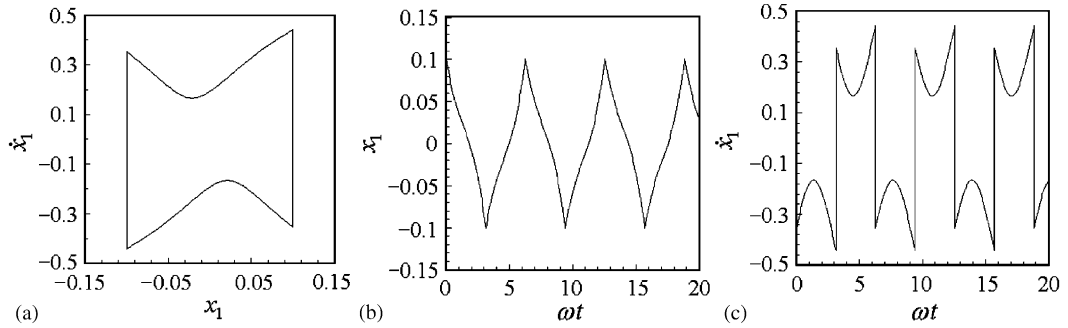

Fig. 3. The phase plane portrait and steady response of the impacting mass $M_1, \omega = 4.0$: (a) phase plane portrait; (b) the steady response $(\omega t, x_1)$; (c) the steady response $(\omega t, \dot{x}_1)$.

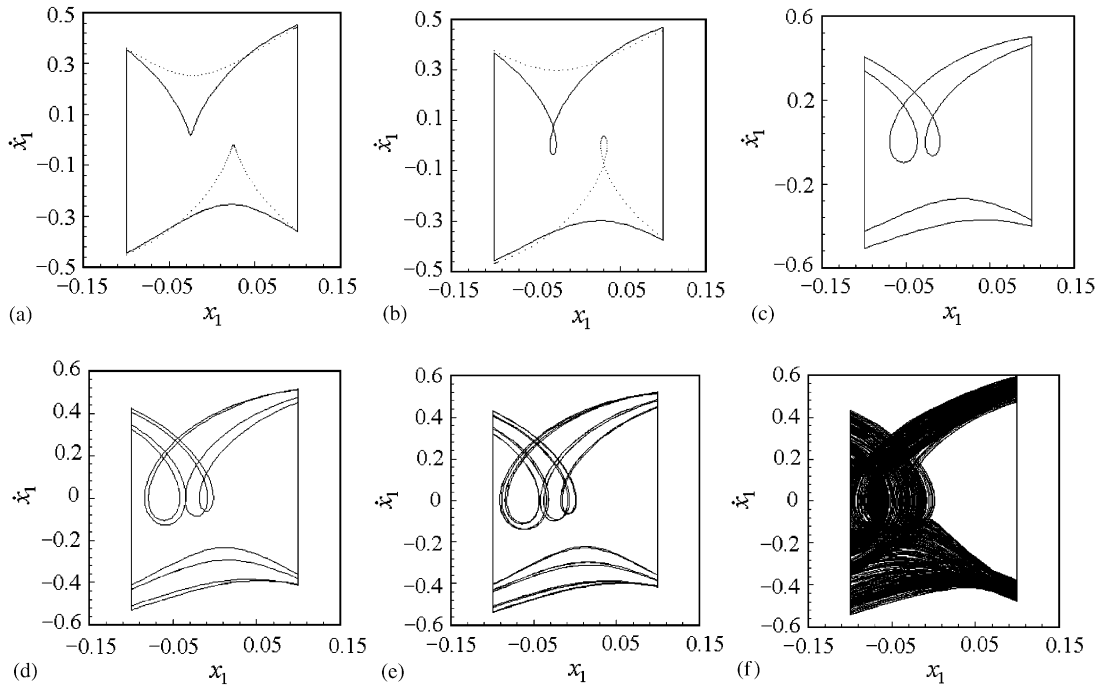

Fig. 4. The phase plane portraits of the impacting mass M_1: (a) pair of antisymmetrical period-one double-impact motions, $\omega = 3.5$; (b) pair of antisymmetrical period-one double-impact motions, $\omega = 3.3$; (c) the 2-2-2 asymmetrical motion, $\omega = 3.1$; (d) the 4-4-4 asymmetrical motion, $\omega = 3.029$; (e) the 8-8-8 asymmetrical motion, $\omega = 2.989$; (f) chaos, $\omega = 2.9$.

system is discontinuous in the case of grazing the stop. Let F_1 represent a resultant force, which consists of spring-restoring force, damping force and sinusoidal excitation acted on the impacting mass M_1, i.e.,

$$F_1 = (x_2 - x_1) + 2\zeta(\dot{x}_2 - \dot{x}_1) + (1 - f_{20}) \sin(\omega t + \tau). \tag{38}$$

If the resultant force F_1, at the instant when the mass M_1 arrives at the right stop A with zero velocity $\dot{x}_1 = 0$, is in the positive direction, i.e.,

$$F_1 = (\bar{x}_{20} - b) + 2\zeta\dot{\bar{x}}_{20} + (1 - f_{20})\sin(\tau) > 0, \tag{39}$$

the force simply pushes the mass M_1 against the stop A, with which it remains in contact. The two-degree-of-freedom vibro-impact system becomes a single-degree-of-freedom oscillator subjected to sinusoidal excitation, and its differential equation of motion is

$$\mu_m\ddot{x}_2 + 2\zeta(1 + \mu_c)\dot{x}_2 + (1 + \mu_k)x_2 - b = f_{20}\sin(\omega t + \tau). \tag{40}$$

Until the resultant force F_1 changes its direction (sign), the force begins to push the mass M_1 away from the stop again, and the single-degree-of-freedom oscillator becomes a two-degree-of-freedom vibro-impact system. In Eq. (39), $\bar{x}_{20}$ and $\dot{\bar{x}}_{20}$ represent, respectively, displacement and velocity of the mass M_2 at the instant when the mass M_1 arrives at the right stop A with zero velocity $\dot{x}_1 = 0$.

If the resultant force F_1 acted on the mass M_1 is in the negative direction immediately after the mass M_1 contacts the right stop A with zero velocity, i.e.,

$$F_1 = (\bar{x}_{20} - b) + 2\zeta\dot{\bar{x}}_{20} + (1 - f_{20})\sin(\tau) < 0, \tag{41}$$

then the force F_1 immediately drives the mass M_1 off the stop. The mass M_1 spends no time stuck to the stop, and moves in opposite direction with initial velocity $\dot{x}_1 = 0$.

A special case must be considered, in which the resultant force F_1 equals zero when the mass M_1 arrives at the stop A with zero velocity. If F_1 changes in positive direction immediately at the instant when the mass contacts the stop A, then the mass M_1 will stick to the stop; otherwise the force F_1 will drive it off the stop immediately.

The system with system parameters (2): $m_2 = 0.6667$, $k_2 = 0.8333$, $b = 0.1$, $R = 0.7$, $f_{20} = 0$ and $\zeta = 0.05$ is chosen for analysis by numerical simulation. When the forcing frequency ω passes through $\omega_c = 3.09227$ by a progressively decreasing way, the period-one double-impact antisymmetrical motions have changed stability, and period-doubling bifurcation of 1-1-1 antisymmetrical motions occur so that 2-2-2 motions have been generated. In Figs. 5(a) and (b) are plotted the global bifurcation diagrams of 1-1-1 symmetrical orbit. There exist two different antisymmetrical 1-1-1 orbits and corresponding diagrams of bifurcation due to different initial conditions, as seen in Figs. 5(a1) and (b1). When the forcing frequency is decreased to $\omega = 2.999$, the system exhibits 2-2-2 motion with "*grazing* the stop", i.e., the mass M_1 begins to touch the stop A with zero velocity ($\dot{x}_{1-} = 0$), which results in singularity of Poincaré map and qualitative changes of the system dynamics. Because of 2-2-2 motion with grazing the stop A, there does not exist 4-4-4 motion bifurcating from 2-2-2 motion with further decrease in the forcing frequency ω, as we will see in Fig. 5. For this reason that the mass's grazing the stop A results in the singularity of Poincaré map, period-doubling bifurcations and dynamic evolution taking place in the vibro-impact system are qualitatively different from those in usual consecutive maps. On grazing boundary of 2-2-2 motion a new impact in the motion period appears and 2-2-3 motion stabilizes. Such a case of transition is shown in Figs. 6(a)–(c), and the phase plane portrait of the 2-2-2 impact motion with grazing the stop A is shown in Fig. 6(b). With further decrease in ω, the

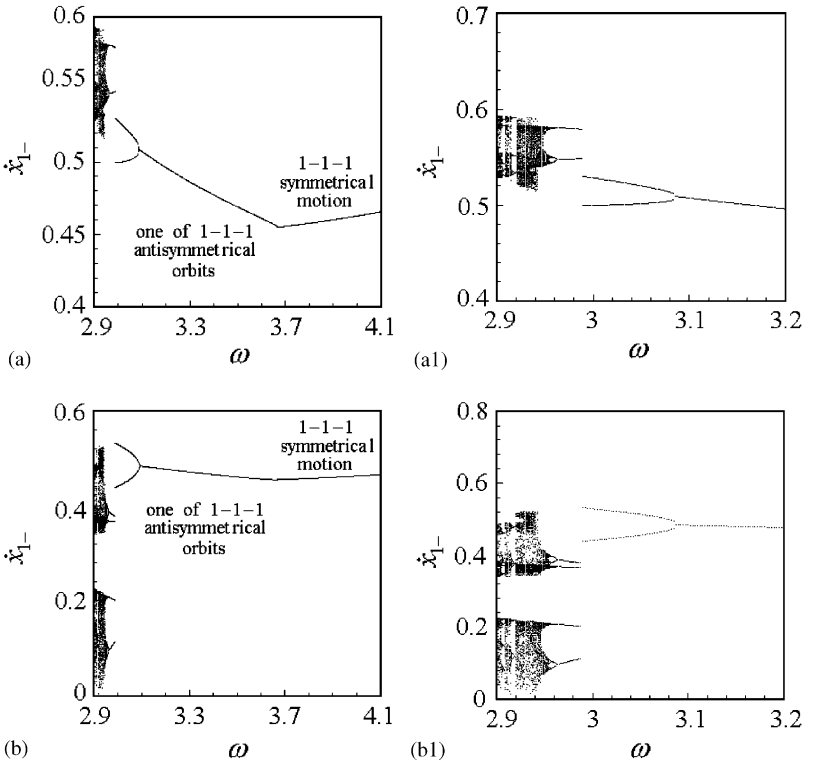

Fig. 5. The global bifurcation diagrams of periodic 1-1-1 motion.

system exhibits stable 2-2-3 impact motion. As ω is decreased to $\omega = 2.989$, a grazing boundary instability of 2-2-3 impact motion appears again, one impact in the motion period appears and the motion transits into 2-2-4 motion. Such a case of transition is similar to the 2-2-2 motion with grazing the stop A. The phase plane portrait of 2-2-4 orbit beyond the grazing boundary is shown in Fig. 6(d). As ω is decreased progressively, the system falls into chaotic motion via period-doubling bifurcation and Feigenbaum period-doubling cascade of 2-2-4 (or 2-4-2) impact orbit. In the route to chaos via period-doubling bifurcation of 1-1-1 antisymmetrical motion, it is possible that grazing bifurcation occur. Grazing bifurcation results in singularity and discontinuity of the Poincaré map so that the period-doubling cascades of 1-1-1 antisymmetrical motions are discontinuous.

The system may exhibit more complicated dynamical behavior in the route to chaos via pitchfork bifurcation of period-one double-impact symmetrical motion. An interesting route from symmetric double-impact orbit to chaos is observed. The system with system parameters (3): $m_2 = 0.3333$, $k_2 = 0.6667$, $b = 2.4$, $\zeta = 0$, $f_{20} = 0$ and $R = 0.8$ is analyzed. When the forcing frequency ω passes through $\omega_c = 1.343812$ by a progressively decreasing way, pitchfork bifurcation of period-one double-impact symmetrical orbit occurs, and the system exhibits the period-one double-impact antisymmetrical motions, see Figs. 7(a), (b) and Fig. 8(a). With decrease in ω, period-doubling bifurcation of 1-1-1 antisymmetrical motion occurs, and the 2-2-2 antisymmetrical motion is generated as seen in Figs. 7(c), (d) and Fig. 8(b). With further decrease

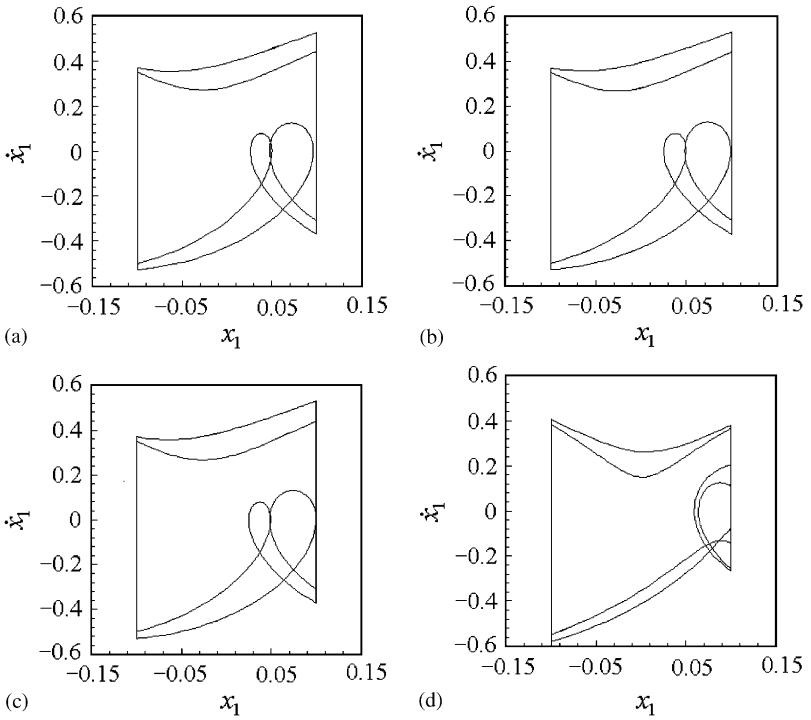

Fig. 6. The phase plane portraits near the grazing boundary: (a) the 2-2-2 motion, $\omega = 3.01$; (b) the 2-2-2 motion on the grazing boundary, $\omega = 2.999$; (c) the 2-2-3 motion beyond the grazing boundary I, $\omega = 2.995$; (d) the 2-2-4 motion beyond the grazing boundary II, $\omega = 2.985$.

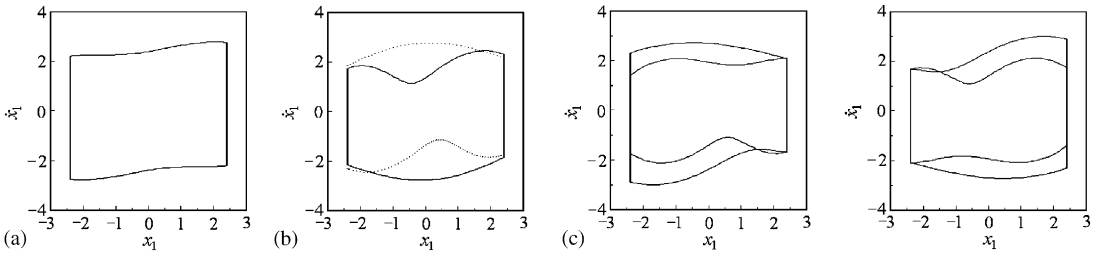

Fig. 7. Phase plane portraits: (a) periodic motion with two symmetrical impacts per force cycle, $\omega = 1.6$; (b) antisymmetrical period 1 double-impact motion, $\omega = 1.31$; (c) periodic 2-2-2 motion, $\omega = 1.309$; (d) periodic 2-2-2 motion; $\omega = 1.309$.

in ω, the 2-2-2 motion will change its stability, and Hopf bifurcation of 2-2-2 motion occurs, see Fig. 8(c). Finally, the system settles into chaotic motion via tori doubling and phase locked as seen in Figs. 8(d)–(h). The chaotic motions of the system, represented by "belt-like" attractor in projected Poincaré sections, are shown in Figs. 8(f)–(h), and the width of "belt-like" attractors increases with decrease in the forcing frequency ω. It is seen that period-doubling bifurcation of 1-1-1 antisymmetrical motion occurs in the example, but no period-doubling cascade emerges because of Hopf bifurcation of 2-2-2 motion.

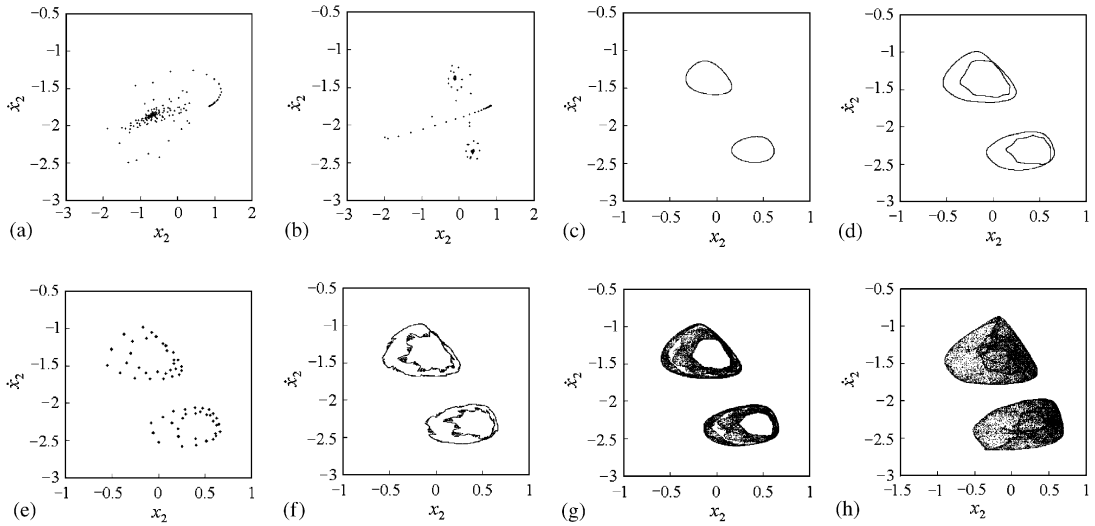

Fig. 8. The projected Poincaré section of the vibro-impact system: (a) the map procedure from unstable 1-1-1 symmetrical motion to stable 1-1-1 antisymmetrical motion, $\omega = 1.31$; (b) the route of unstable 1-1-1 motion to stable 2-2-2 antisymmetrical motion, $\omega = 1.309$; (c) the attracting invariant circles of 2-2-2 points (quasi-periodic impact motion), $\omega = 1.3067$; (d) the torus doubling, $\omega = 1.305815$; (e) phase locked, $\omega = 1.30573805$; (f) chaos, $\omega = 1.30567$; (g) chaos, $\omega = 1.3056$; (h) chaos, $\omega = 1.3048$.

6. Hopf bifurcation of periodic motion with two symmetrical impacts per force cycle

Shaw [24,25] studied dynamics of a single-degree-of-freedom system having symmetrically placed rigid stops and subjected to periodic excitation, and found that no Hopf bifurcation of symmetrical double-impact motion occurs for the system. However it is found that there exists Hopf bifurcation of symmetrical double-impact motion for the two-degree-of-freedom vibro-impact system shown in Fig. 1. By computing and analyzing the eigenvalues of $Df(\omega, 0)$, we can find Hopf intersecting conditions of 1-1-1 symmetrical motion of the vibro-impact system. The system, with system parameters (4): $m_2 = 0.8$, $k_2 = 0.8333$, $b = 0.25$, $R = 0.8$, $f_{20} = 0$ and $\zeta = 0.0075$, is considered. The eigenvalues of $Df(\omega, 0)$ are computed with $\omega \in [2.9, 3.2]$. When the forcing frequency ω is on the interval $\omega \in [2.9, 3.05639)$, all eigenvalues of $Df(\omega, 0)$ stay strictly inside the unit circle. As $\omega = \omega_c = 3.05639$, $Df(\omega, 0)$ has a complex conjugate pair of eigenvalues $\lambda_{1,2}(\omega_c)$ on the unit circle, while the remainder of eigenvalues are still inside the unit circle. The complex conjugate pair of eigenvalues $\lambda_{1,2}(\omega_c)$ will cross the unit circle correspondingly, and the other eigenvalues will still stay inside the unit circle as ω passes through ω_c . It is possible that Hopf bifurcation of 1-1-1 symmetrical motion occur for $\omega > \omega_c$. The theoretical analyses of the example are well supported by numerical results below. The Poincaré section is taken in the form σ, which will be four dimensional. The section is then projected to the $(x_2, \dot{x}_2)$ or (τ, x_2) plane, etc., which is called the projected Poincaré section. A theoretical fixed point of 1-1-1 symmetrical impact motion, with corresponding forcing frequency ω, is taken as an initial map point. Route from quasi-periodic impact to chaos via phase locked is shown in Fig. 9. It is shown by the

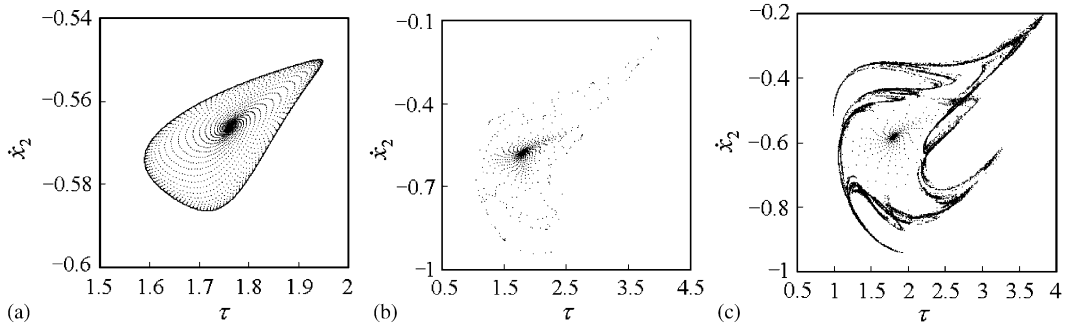

Fig. 9. The projected Poincaré section: (a) the attracting invariant circle of 1-1-1 symmetrical point (quasi-periodic impact motion), $\omega = 3.062$; (b) phase locked, $\omega = 3.09$; (c) chaos, $\omega = 3.12$.

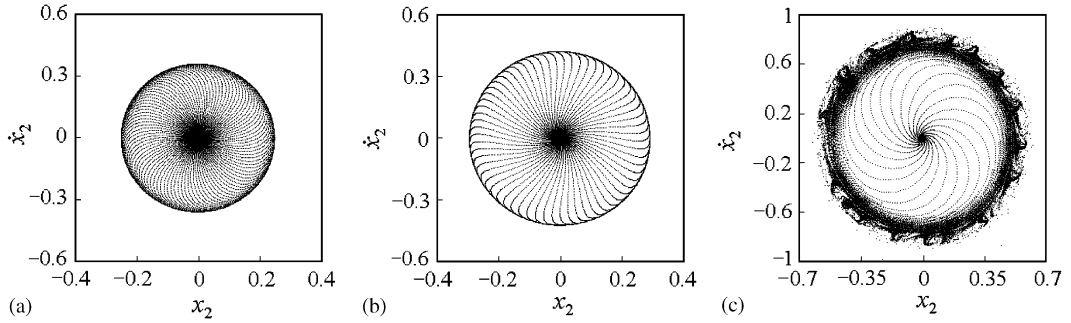

Fig. 10. The projected Poincaré section: (a) the attracting invariant circle of 1-1-1 point (quasi-periodic impact motion), $\omega = 5.73$; (b) the attracting invariant circle, $\omega = 5.7$; (c) the route from unstable 1-1-1 point to chaos via a quasi-attracting invariant circle, $\omega = 5.5$.

numerical results that the system exhibits stable period-one double-impact symmetrical motion with $\omega \in [2.9, 3.05639)$, which is represented by a stable fixed point in the projected Poincaré sections. As expected, a quasi-periodic response, represented by the attracting invariant circle shown in Fig. 9(a), appears at $\omega = 3.062$, just after the Hopf bifurcation value $\omega = 3.05639$. It is to be noted that the quasi-periodic attractor, which is identified by a closed curve in the projected Poincaré section, is smooth in nature near the bifurcation point. As the value of ω moves further away from the Hopf bifurcation value, the invariant circle expands, and the smoothness of the quasi-periodic attractor is changed by degrees until it is destroyed. With further increase in ω, phase locked takes place so that the quasi-periodic motion gets locked into a periodic attractor of higher (than the basic) period, which subsequently becomes unstable and chaotic. A periodic attractor is shown for $\omega = 3.09$ in Fig. 9(b). The chaotic motion of the system, represented by "belt-like" attractor in projected Poincaré section, is shown in Fig. 9(c).

The vibro-impact system with system parameters (5): $m_2 = 0.5$, $\mu_k = 0.5146$, $b = 0.1$, $R = 0.8$, $f_{20} = 0$, and $\zeta = 0.0025$ has been chosen for analysis. When the forcing frequency ω passes through the critical value $\omega_c = 5.78862$ decreasingly, $Df(\omega, 0)$ has a complex conjugate pair of eigenvalues $\lambda_{1,2}(\omega_c)$ escaping correspondingly the unit circle, the remainder of eigenvalues are still

inside the unit circle. This means that Hopf bifurcation of 1-1-1 symmetrical motion occurs for $\omega<\omega_c$. The quasi-periodic impact motion, represented by the attracting invariant circle in projected Poincaré section, are plotted for $\omega = 5.73$ and $\omega = 5.7$ in Figs. 10(a) and (b). With decrease in ω, the system falls into chaotic motion via a quasi-attracting invariant circle [15]. The quasi-attracting invariant circle is attracting for the map point inside the circle, and repelling for the map point outside it. The route, from unstable 1-1-1 symmetrical motion to chaos via the quasi-attracting invariant circle, is shown for $\omega = 5.5$ in Fig. 10(c).

7. The influence of system parameters on periodic motions and bifurcations

The two-degree-of-freedom model studied here involves seven system parameters: $\omega, m_2, k_2, f_{20}, R, \zeta$ and b. Due to this relatively large number of parameters the detailed influence of each parameter on the system dynamics is not presented here. However, it is of special interest to acquire an overall picture of the system dynamics for some extreme values of parameters, especially those which relate to the degenerated case of a single-degree-of-freedom system. Taking system parameters: $m_2 = 0.5$, $k_2 = 0.5$, $R = 0.8$, $\zeta = 0.1$, $b = 0.1$ and $f_{20} = 0$, as the criterion parameters, we analyze the influence of system parameters on the system dynamics. Thus, in Figs. 11 and 12 some bifurcations diagrams corresponding to some extreme parameter values are presented. Only changed parameter is given in Figs. 11(b)–(j) and 12, and all the other parameters, not given, are the same as criterion parameters. In most case one observes the typical behavior, from Figs. 11 and 12, that period-one double-impact symmetrical motion generally undergoes pitchfork bifurcation with decrease in ω. Hopf bifurcation of the motion occurs only in the case of larger values b or lower damping. Period-one double-impact antisymmetrical motion will undergo different types of bifurcations according to variation of system parameters. The bifurcation diagram, corresponding to the criterion parameters, is shown in Fig. 11(a). Hopf bifurcation of period-one double-impact antisymmetrical motion occurs with decrease in the forcing frequency. When the coefficient of restitution is low, Fig. 11(b), the 4-4-4 motion exists over a region of low forcing frequencies, and the region of chaotic motion become smaller. The chaotic region shrinks, and saddle–node bifurcation of period-one double-impact antisymmetrical motion will occur as ω is changed decreasingly. Low damping, Fig. 11(c), leads to enlarged areas of chaotic motions, and Hopf bifurcation of period-one double-impact symmetrical motion occurs with decrease in ω. There exists also the period-one double-impact symmetrical motion in another relatively narrow range of the forcing frequency separated by two regions of other periodic and chaotic motions, of which pitchfork bifurcation is created with decrease in ω. Saddle–node bifurcation of period-one double-impact antisymmetrical motion will occur for large damping as ω is changed decreasingly, see Fig. 11(d). For low m_2 and large k_2 the behavior is similar to that of a one-degree-of-freedom system (in the appendix), as seen in Figs. 11(e) and (h), respectively. Period-doubling bifurcation of period-one double-impact antisymmetrical motion may be observed obviously in the two bifurcation diagrams. When m_2 becomes larger the period-doubling bifurcation associated with period-one double-impact antisymmetrical motion occurs; see Fig. 11(f). When k_2 becomes smaller, the system may exhibit period-one double-impact antisymmetrical motion in two different internals of forcing frequency, and Hopf bifurcation of the periodic motion occurs in the first internal and period-doubling bifurcation does in the second with decrease in ω; see Fig. 11(g).

This represents a system with a very stiff spring between the masses. When f_{20} increases, the chaotic region shrinks, and period-doubling bifurcation of period-one double-impact antisymmetrical motion will take place as ω is changed by a progressively decreasingly way; see Figs. 11(i) and (j). The values of f_{20} influence the impact velocities significantly. Large values of f_{20} will result in low impact velocities. The phenomena become more pronounced when the value of f_{20} is larger.

The clearance is the most important system parameter for the non-linear system shown in Fig. 1. Studying the influence of the clearance, one finds that, smaller values of b generally lead to enlarged areas of the chaotic motions as seen in Fig. 12(a), and the period-one double-impact

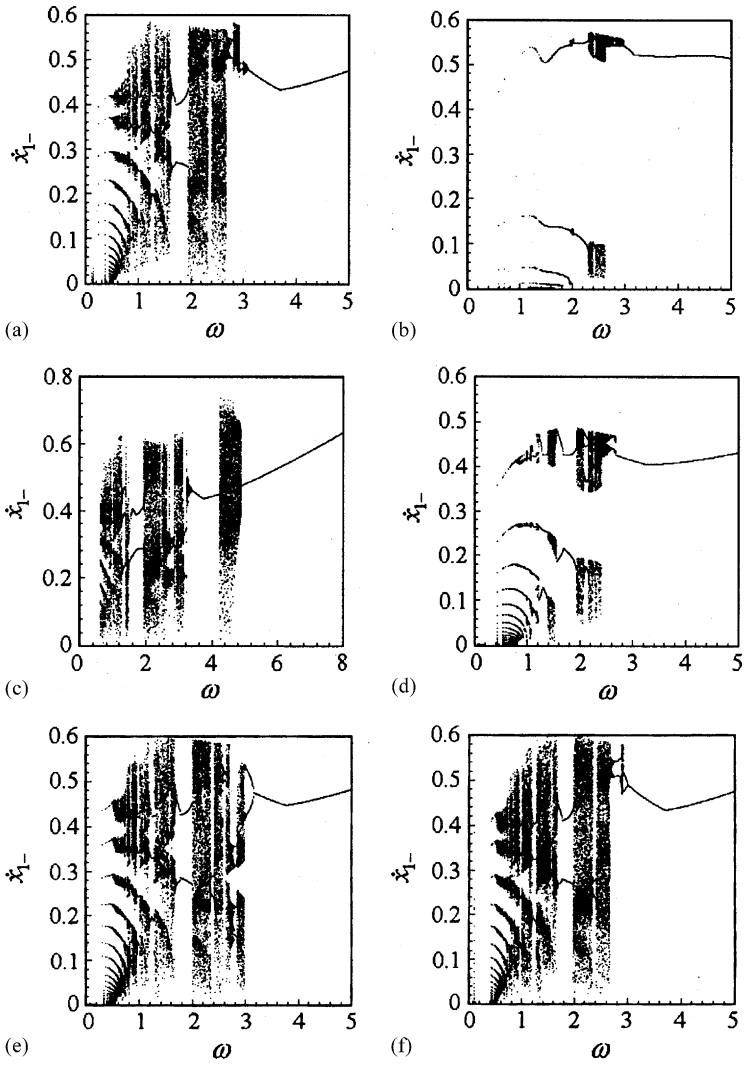

Fig. 11. Bifurcation diagrams for the impact velocity of the impacting mass: (a) $m_2 = 0.5$, $k_2 = 0.5$, $f_2 = 0$, $b = 0.1$, $\zeta = 0.1$, $R = 0.8$; (b) $R = 0.3$; (c) $\zeta = 0.01$; (d) $\zeta = 0.6$; (e) $m_2 = 0.1$; (f) $m_2 = 0.99$; (g) $k_2 = 0.01$; (h) $k_2 = 0.9$; (i) $f_2 = 0.3$; (j) $f_2 = 0.6$.

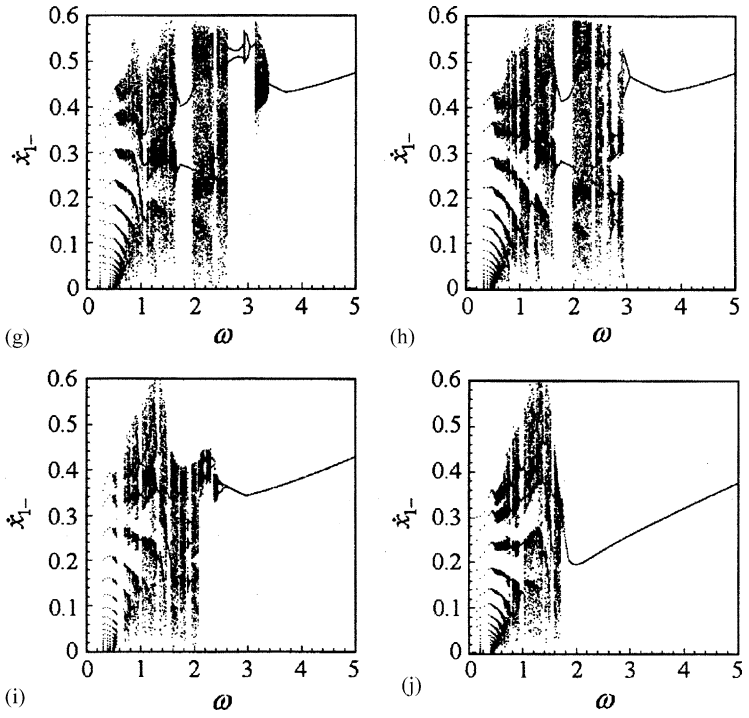

Fig. 11 (*continued*).

antisymmetrical motion will undergo period doubling bifurcation with gradual decrease in ω. When b further decreases, the window of periodic 1-1-1 motion moves towards higher frequencies. Moreover, smaller values of b result in lower impact velocities. When b is changed increasingly, the chaotic regions shrinks gradually, and the period-one double-impact antisymmetrical motion will undergo saddle–node bifurcation as the forcing frequency is decreased; see Figs. 12(b)–(e). For large values of b, the chaotic motion exists over the relatively narrow frequency range shown in Figs. 12(f)–(h). The behavior is similar to that of a one-degree-of-freedom system (see Figs. 17(g)–(i) in the appendix). With gradual decrease in ω, the period-one double-impact symmetrical motion of the two-degree-of-freedom vibratory system with symmetrical rigid stops will generally undergo Hopf bifurcation in the case of large values of b. However, for larger values of b the mass M_1 cannot hit the stops, and the system will undergo simple oscillations and behave as a linear system.

In most cases one observes the windows of period-one four-impact symmetrical motions, separated by other periodic or chaotic regions, in the bifurcation diagrams. The period-one four-impact symmetrical motion exists over the relatively narrow forcing frequency range; see Figs. 11(a)–(h) and 12(a)–(e). Following the steady state motion as ω decreases, it is seen that a supercritical pitchfork bifurcation generally occurs, which results in the creation of a pair of antisymmetrical four-impact period-one motions. These motions, in most cases, then each undergo a succession of period doubling, which eventually result in apparently non-periodic, or chaotic motions. Here the system with criterion parameters is chosen for analysis. Representative orbits are shown in Figs. 13 and 14. The stable 1-2-2 symmetrical motion exists in the frequency

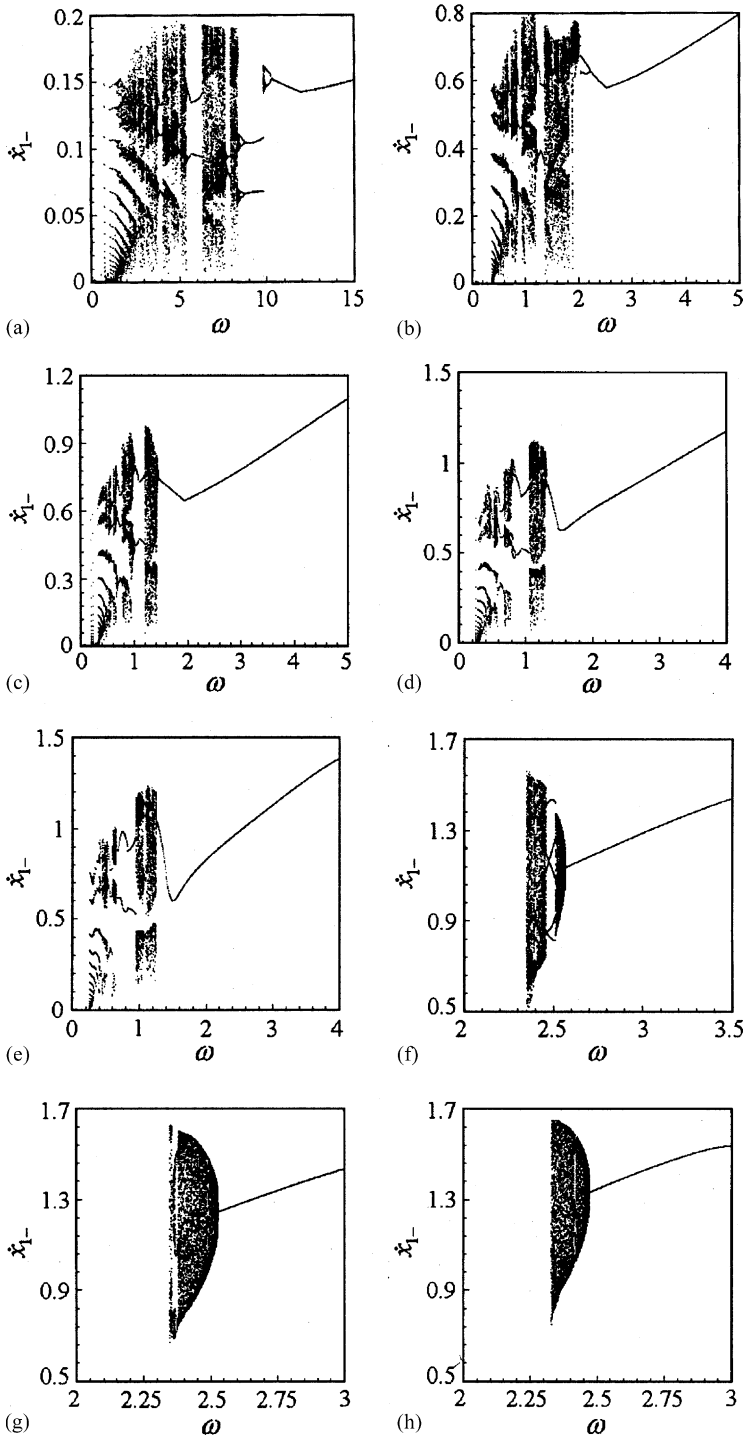

Fig. 12. The global bifurcation diagrams for the impact velocity of the impacting mass; (a) $b = 0.01$; (b) $b = 0.2$; (c) $b = 0.3$; (d) $b = 0.4$; (e) $b = 0.5$; (f) $b = 0.6$; (g) $b = 0.7$; (h) $b = 0.8$.

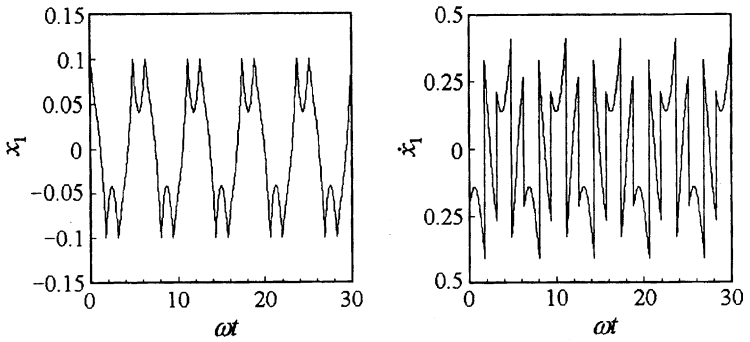

Fig. 13. The steady response of the impacting mass M_1, 1-2-2 symmetrical motion, $\omega = 1.85$.

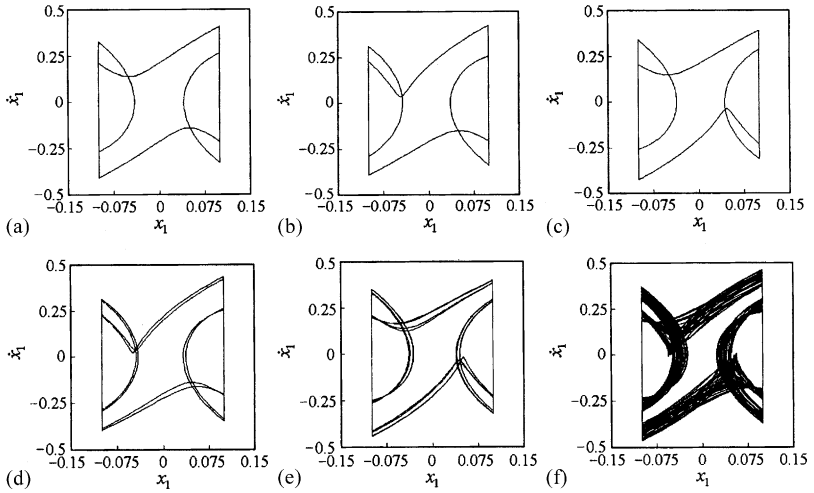

Fig. 14. The phase plane portraits of the impacting mass M_1: (a) 1-2-2 symmetrical motion, $\omega = 1.85$; (b) 1-2-2 antisymmetrical motion, $\omega = 1.65$; (c) 1-2-2 antisymmetrical motion, $\omega = 1.65$; (d) 2-4-4 motion, $\omega = 1.635$; (e) 4-8-8-motion, $\omega = 1.624$; (f) chaos, $\omega = 1.6$.

range $\omega \in (1.7125, 1.975)$. At $\omega = 1.7125$, two new antisymmetrical motions, each having period one and four impacts, appear as the symmetrical motion becomes unstable; see Figs. 14(b) and (c). This means that a supercritical pitchfork bifurcation of the symmetrical motion occurs at the value of forcing frequency. Period doubling bifurcation of the antisymmetrical motion occurs as the forcing frequency varies decreasingly, and the system eventually falls into apparently non-periodic, or chaotic motions via the period doubling sequences; see Figs. 14(d)–(f).

An observation of interest is the existence of Hopf bifurcation of period-one double-impact antisymmetrical motion in bifurcation diagrams shown in Figs. 11(a), (c) and (g). A representative quasi-periodic motion corresponding to Fig. 11(g) is shown in Figs. 15(a) and (b). The quasi-periodic impact motion finally transits to chaos via phase locked as ω is changed decreasingly; see Figs. 15(c) and (d). It is found that there exists not only Hopf bifurcation associated with

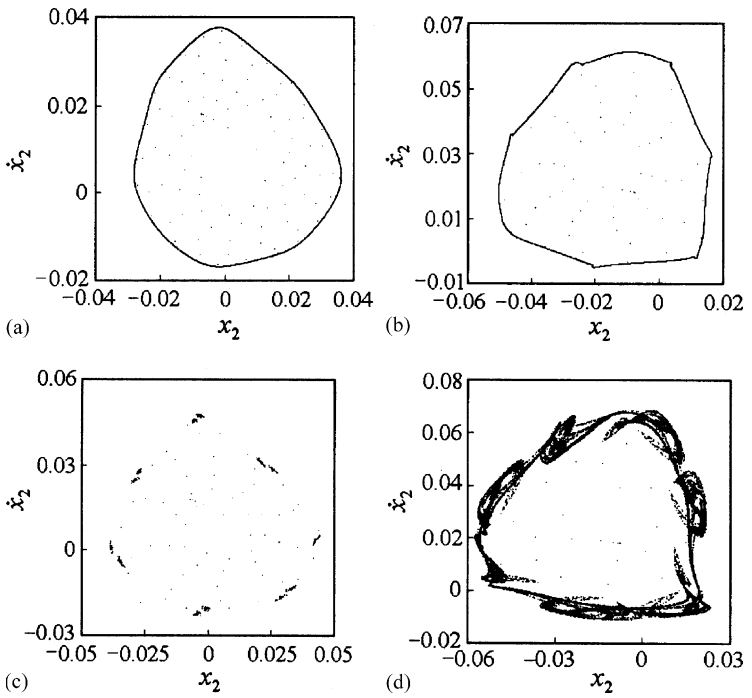

Fig. 15. The projected Poincaré section: (a) the attracting invariant circle of 1-1-1 antisymmetrical point, $\omega = 3.35$; (b) the attracting invariant circle of 1-1-1 antisymmetrical point, $\omega = 3.33$; (c) phase locked, $\omega = 3.32$; (d) chaos, $\omega = 3.3$.

period-one double-impact symmetrical motion, but also Hopf bifurcation of period-one double-impact antisymmetrical motion occurs in the non-linear system shown in Fig. 1.

The similarities with the one-degree-of-freedom system can especially be found in the two cases of low m_2 (Fig. 11(e)) or large k_2 (Fig. 11(h)). These results are in agreement with the results presented in Fig. 15(a) of the appendix for single-degree-of-freedom system having symmetrically placed rigid stops. The similarities with the one-degree-of-freedom system, in the case of large ζ, can also be observed in Figs. 11(d) and 7(c) (in the appendix). Moreover, a common characteristic, for the one or two degree of freedom systems, is that large values b generally lead to narrow areas of chaotic motion and high impact velocities. Similarities in bifurcations can be observed by comparing Figs. 11, 12 and 17. The two-degree-of-freedom system shows bifurcations similar to those of one-degree-of-freedom system: pitchfork bifurcation of symmetrical two-impact motion, period doubling and saddle–node bifurcations of antisymmetrical two-impact motion, grazing bifurcation. However, there are some significant deviations, and important differences in system behavior at some extreme values of the parameters. Such cases are low values of ζ (Fig. 11(c)) or k_2 (Fig. 11(g)) and high values of f_{20} (Fig. 12(j)). The second case is high stiffness of the spring between the masses compared to the spring attached to the wall. Besides the deviations mentioned above, there is also a significant difference in bifurcation behavior. No Hopf bifurcation occurs in the one-degree-of-freedom vibrating system with symmetrical rigid stops.

8. Conclusions

A two-degree-of-freedom system having symmetrically placed rigid stops and subjected to periodic excitation is considered. An important application where the model studied here may be of use is in the dynamics of heat exchanger tubes in nuclear reactors [23]. Such tubes are designed to have clearances at support points to allow for thermal expansion. When fluid flows past these tubes vortex shedding occurs and the tubes are excited. The response of such systems is very complicated [23] and the wearing of these tubes is a major problem in the nuclear industry. Fluid flow past panels and beams can result in chaotic motions and thus bifurcation behavior and chaotic motions may provide an appropriate tool in the study of tube wear. Stability, pitchfork and Hopf bifurcations of period-one double-impact symmetrical motion of the system with symmetrical rigid stops are analyzed in the paper. Routes of 1-1-1 symmetrical motions to chaos are observed by numerical simulation.

When the pitchfork bifurcation occurs, the period-one double-impact symmetrical motion will change its stability and a pair of period-one double-impact antisymmetrical motions are born. There exist two different 1-1-1 antisymmetrical orbits and corresponding diagrams of bifurcation due to different initial conditions. With decrease in the forcing frequency ω, the 1-1-1 antisymmetrical motions will lose stability, these motions then each undergo a succession of period doubling bifurcations, which eventually result in apparently nonperiodic, or chaotic motions.

There exist the motions with grazing the stop in the route to chaos, which cause singularities of Poincaré map. A new impact in the motion period usually appears or vanishes on the grazing boundary so that the period-doubling cascades of 1-1-1 antisymmetrical motions are discontinuous.

Interesting features like Hopf bifurcation of 2-2-2 motion, torus bifurcation and phase locked are found in the route to chaos via pitchfork bifurcation of 1-1-1 symmetrical motion. This is one of non-typical routes to chaos.

No Hopf bifurcation of symmetrical double-impact motion occurs in a single degree-of-freedom system having symmetrically placed rigid stops and subjected to periodic excitation [24,25]. However, Hopf bifurcations of 1-1-1 symmetrical and asymmetrical motions are shown to exist in the two-degree-of-freedom vibro-impact system with symmetrical rigid stops. As the forcing frequency is changed, the quasi-periodic impact motion may lead to chaos via torus bifurcation, phase locked or quasi-attracting invariant circle.

The similarities with the one-degree-of-freedom system are found in the two cases of low m_2, large k_2. The similarities, in system behavior, can also be observed in the case of large ζ. Besides the cases mentioned above, a common characteristic, for the one- or two-degree-of-freedom systems with symmetrical rigid stops, is that large values of b generally lead to narrow areas of chaotic motion and high impact velocities. For larger values of b the mass M_1 cannot hit the stops, and the system will undergo simple oscillations and behave as a linear system. However, there are some significant deviations, and important differences in system behavior at some extreme values of the parameters. Such cases are low values of ζ, low values of k_2 or high values of f_{20}.

Acknowledgements

The authors gratefully acknowledge the support by the National Science Foundation of China (10172042, 10072051), Special Foundation of Railway (J99Z100) and the Provincial Science Foundation of Gansu (ZS011-A25-010-Z), China.

Appendix A

A one-degree-of-freedom system having symmetrically placed rigid stops and subjected to periodic excitation is shown in Fig. 16.

Between the stops, the non-dimensional differential equations of motion are given by

$$\ddot{x} + 2\zeta\dot{x} + x = \sin(\omega t + \tau), \quad |x| < b.$$

When the impacts occur, for $|x| = b$, the velocities of the impacting mass M are changed according to the impact law

$$\dot{x}_{A+} = -R\dot{x}_{A-} \quad (x_1 = b), \quad \dot{x}_{C+} = R\dot{x}_{C-} \quad (x_1 = -b).$$

In these relations we have used the non-dimensional quantities

$$\omega = \Omega\sqrt{\frac{M}{K}}, \quad t = T\sqrt{\frac{K}{M}}, \quad \zeta = \frac{C_1}{2\sqrt{KM}}, \quad b = \frac{BK}{P}, \quad x = \frac{KX}{P}.$$

The Poincaré section is $\sigma = \{(x, \dot{x}, \theta) \in \mathbf{R}^2 \times \mathbf{S}, x = b, \dot{x} = \dot{x}_+\}$.

The system parameters $b = 0.1, \zeta = 0.1$ and $R = 0.8$ are taken as the criterion parameters; the influence of system parameters such as the damping ratio and clearance on the system dynamics is analyzed. The bifurcation diagrams for the impact velocity of the impacting mass are shown in Fig. 17. Only changed parameter is given in Figs. 17(b)–(i), and all the other parameters, not given, are the same as the criterion parameters.

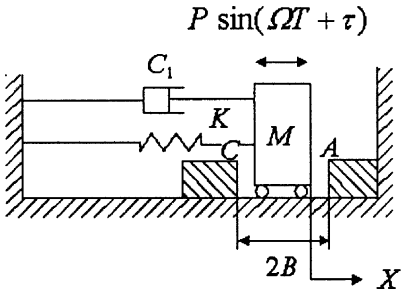

Fig. 16. The schematic of a one-degree-of-freedom vibratory system with symmetrical rigid stops.

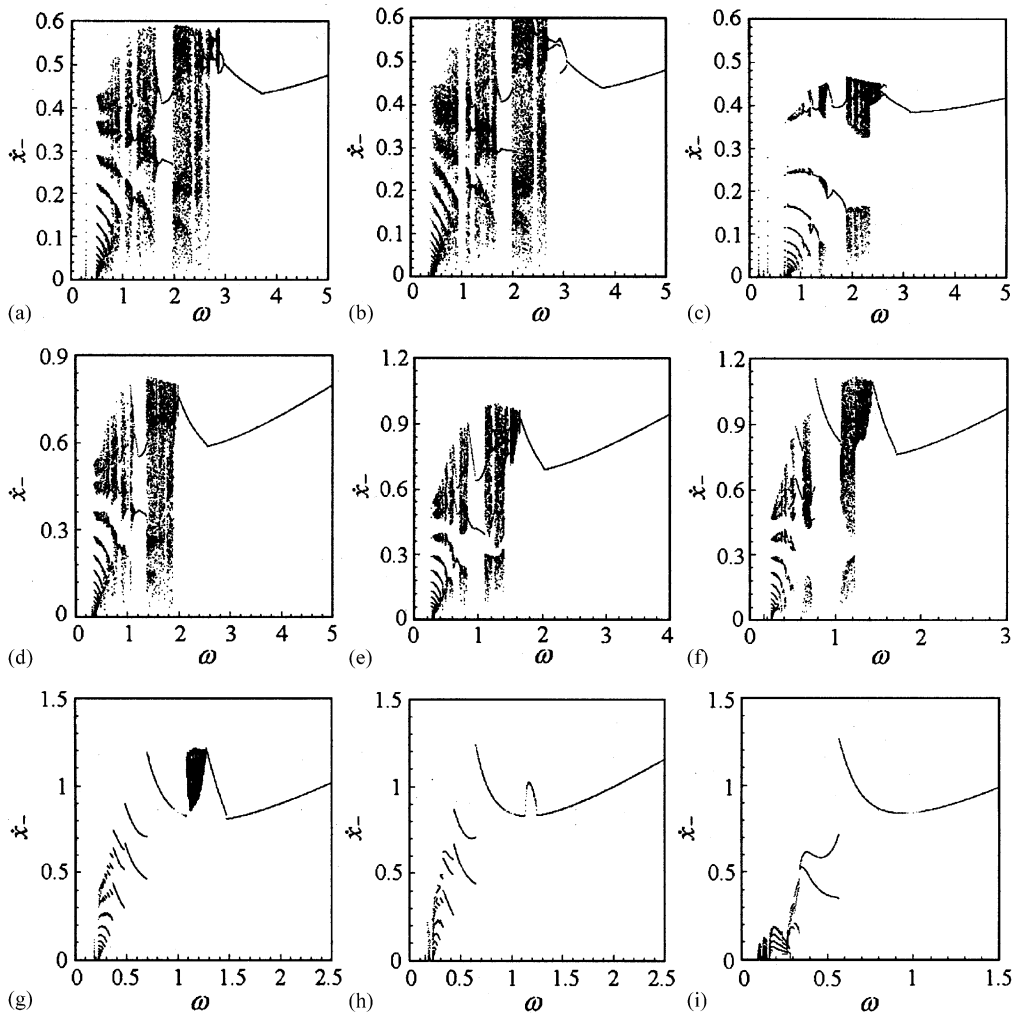

Fig. 17. The bifurcation diagrams for the impact velocity of the impacting mass: (a) $b = 0.1$, $\zeta = 0.1$, $R = 0.8$; (b) $\zeta = 0.01$; (c) $\zeta = 0.6$; (d) $b = 0.2$; (e) $b = 0.3$; (f) $b = 0.4$; (g) $b = 0.5$; (h) $b = 0.6$; (i) $b = 0.8$.

References

[1] P.J. Holmes, The dynamics of repeated impacts with a sinusoidally vibrating table, *Journal of Sound and Vibration* 84 (1982) 173–189.

[2] S.W. Shaw, P.J. Holmes, A periodically forced piecewise linear oscillator, *Journal of Sound & Vibration* 90 (1983) 129–155.

[3] S.W. Shaw, P.J. Holmes, Periodically forced linear oscillator with impacts: chaos and long-period motions, *Physical Review Letters* 51 (1983) 857–894.

[4] J.M.T. Thompson, R. Ghaffari, Chaos after period-doubling bifurcations in the resonance of an impact oscillator, *Physics Letters A* 91 (1984) 5–8.

[5] J.O. Aidanpää, B.R. Gupta, Periodic and chaotic behaviour of a threshold-limited two-degree-of-freedom system, *Journal of Sound and Vibration* 165 (1993) 305–327.

[6] G.S. Whiston, Singularities in vibro-impact dynamics, *Journal of Sound and Vibration* 152 (1992) 427–460.
[7] A.B. Nordmark, Non-periodic motion caused by grazing incidence in an impact oscillator, *Journal of Sound and Vibration* 145 (1991) 279–297.
[8] M.I. Feigin, The increasingly complex structure of the bifurcation tree of a piecewise-smooth system, *Journal of Applied Mathematics and Mechanics* 59 (1995) 853–863.
[9] A.P. Ivanov, Bifurcation in impact systems, *Chaos, Solitons & Fractals* 7 (1996) 1615–1634.
[10] F. Peterka, Bifurcation and transition phenomena in an impact oscillator, *Chaos, Solitons & Fractals* 7 (1996) 1635–1647.
[11] S. Natsiavas, Dynamics of multiple-degree-of-freedom oscillators with colliding components, *Journal of Sound and Vibration* 165 (1993) 439–453.
[12] S. Chatterjee, A.K. Mallik, Bifurcations and chaos in autonomous self-excited oscillators with impact damping, *Journal of Sound and Vibration* 191 (1996) 539–562.
[13] S. Chatterjee, A.K. Mallik, Three kinds of intermittency in a nonlinear mechanical system, *Physical Review E* 53 (1996) 4362–4367.
[14] C. Budd, F. Dux, A. Cliffe, The effect of frequency and clearance variations on single-degree-of-freedom impact oscillators, *Journal of Sound and Vibration* 184 (1995) 475–502.
[15] G.W. Luo, J.H. Xie, Hopf bifurcation of a two-degree-of-freedom vibro-impact system, *Journal of Sound and Vibration* 213 (1998) 391–408.
[16] G.W. Luo, J.H Xie, Hopf bifurcations and chaos of a two-degree-of-freedom vibro-impact system in two strong resonance cases, *International Journal of Nonlinear Mechanics* 37 (2002) 19–34.
[17] C.K. Sung, W.S. Yu, Dynamics of a harmonically excited impact damper: bifurcations and chaotic motion, *Journal of Sound and Vibration* 158 (1992) 317–329.
[18] Hu Haiyan, Controlling chaos of a periodically forced nonsmooth mechanical system, *Acta Mechanica Sinica* 11 (1995) 251–258.
[19] J.D. Weger, V.D. Water, Control of impact dynamics by means of a reduced map, in: D.H. van Campen (Ed.), *Proceeding of IUTAM Symposium on Interaction Between Dynamics and Control in Advanced Mechanical Systems*, Kluwer Academic Publishers, Dordrecht, 1996.
[20] J.P. Mejaard, A.D. De Pater, Railway vehicle systems dynamics and chaotic vibrations, *International Journal of Nonlinear Mechanics* 24 (1989) 1–17.
[21] A. Kahraman, R. Singh, Non-linear dynamics of a geared rotor-bearing system with multiple clearances, *Journal of Sound and Vibration* 144 (1991) 469–506.
[22] A. Kunert, F. Pfeiffer, Stochastic model for rattling in gear-boxes, in: W. Schiehlen (Ed.), *Nonlinear Dynamics in Engineering System*, IUTAM, Germany, August 21–25, 1989, pp. 173–180.
[23] R.J. Rogers, R.J. Pick, On the dynamic spatial response of a heat exchanger tube with intermittent baffle contacts, *Nuclear Engineering and Design* 36 (1976) 81–90.
[24] S.W. Shaw, The dynamics of a harmonically excited system having rigid amplitude constraints, Part 1: subharmonic motions and local bifurcations, *Journal of Applied Mechanics* 52 (1985) 453–458.
[25] S.W. Shaw, The dynamics of a harmonically excited system having rigid amplitude constraints, Part 2: chaotic motions and global bifurcations, *Journal of Applied Mechanics* 52 (1985) 459–464.